Carbon-Nanotube-Modified Electrodes for Highly Efficient Acute Neural Recording

Jung Hwal Shin, Guk Bae Kim, Eun Joo Lee, Taechang An, Kumjae Shin, Seung Eun Lee, WooSeok Choi, Sukchan Lee, Charles Latchoumane, Hee-Sup Shin, and Geunbae Lim**

Microelectrodes are widely used for monitoring neural activities in various neurobiological studies. The size of the neural electrode is an important factor in determining the signal-to-noise ratio (SNR) of recorded neural signals and, thereby, the recording sensitivity. Here, it is demonstrated that commercial tungsten microelectrodes can be modified with carbon nanotubes (CNTs), resulting in a highly sensitive recording ability. The impedance with the respect to surface area of the CNT-modified electrodes (CNEs) is much less than that of tungsten microelectrodes because of their large electrochemical surface area (ESA). In addition, the noise level of neural signals recorded by CNEs is significantly less. Thus, the SNR is greater than that obtained using tungsten microelectrodes. Importantly, when applied in a mouse brain invivo, the CNEs can detect action potentials five times more efficiently than tungsten microelectrodes. This technique provides a significant advance in the recording of neural signals, especially in brain regions with sparse neuronal densities.

1. Introduction

Microelectrodes for neural recording have been developed over a span of 50 years using various materials such as tungsten, silicon,[1,2] ceramics,[3,4] and flexible substrates,[5–7] and with various designs such as single wire, stereotrode,[8,9] tetrode,[10–12] and multiple-site electrode.[13–16]

For extracellular recording of action potentials (APs), neural electrodes should be implanted very close to the target neurons, with minimal damage. Successful recordings depend on many factors, including the impedance and size of the electrode, and the composition of the connective tissue sheath surrounding the electrode during neural recording.[17] A sharp electrode tip and small electrode size can reduce the tissue damage caused by the inserted electrode.[18] On the other hand, a reduction in the size of the tip will increase the impedance between the tip and the tissue, resulting in reduced recording sensitivity.[19] Thus, to achieve a high recording sensitivity with minimal damage, we need to develop a small-scale neural electrode with low impedance.

Recently, carbon nanotubes (CNTs) have become popular as a material for neural electrodes owing to their high electrochemical surface area (ESA)/geometric surface area (GSA) ratio, which is a property that is inherent to nanotube geometry.[17] Additionally, CNTs can be modified to improve their biocompatibility and other functional properties.[20,21] Because a CNT probe is a nanometer-scale needle with a very small tip, it has also been applied widely for intracellular analysis,[22,23] neural signal measurements,[24,25] and scanning electrochemical microscopy (SECM)[26,27] with greater spatial resolution. In a brain, a CNT probe with high spatial resolution could have high selectivity to individual neurons.

J. H. Shin, K. Shin, Dr. W. Choi, Prof. G. Lim
Department of Mechanical Engineering
Pohang University of Science and Technology (POSTECH)
Pohang 790–784, Republic of Korea
E-mail: limmems@postech.ac.kr
J. H. Shin, Dr. S. Lee, Dr. C. Latchoumane, Dr. H.-S. Shin
Center for Cognition and Sociality
Institute for Basic Science (IBS)
Daejeon 305–811, Republic of Korea
E-mail: shin@ibs.re.kr
Dr. G. B. Kim
Interaction and Robotics Research Center
Korea Institute of Science and Technology (KIST)
Seoul 136–791, Republic of Korea
Dr. E. J. Lee
School of Interdisciplinary Bioscience and Bioengineering
POSTECH, Pohang 790–784, Republic of Korea
Prof. T. An
Department of Mechanical Design Engineering
Andong National University
Andong 760–749, Republic of Korea
S. E. Lee
Center for Functional Connectomics
Brain Science Institute
KIST, Seoul 136–791, Republic of Korea
Dr. H.-S. Shin
Department of Neuroscience
University of Science & Technology (UST)
Daejon 305–333, Republic of Korea
Prof. G. Lim
Department of Integrative Bioscience and Biotechnology
POSTECH, Pohang 790–784, Republic of Korea

DOI: 10.1002/adhm.201300183

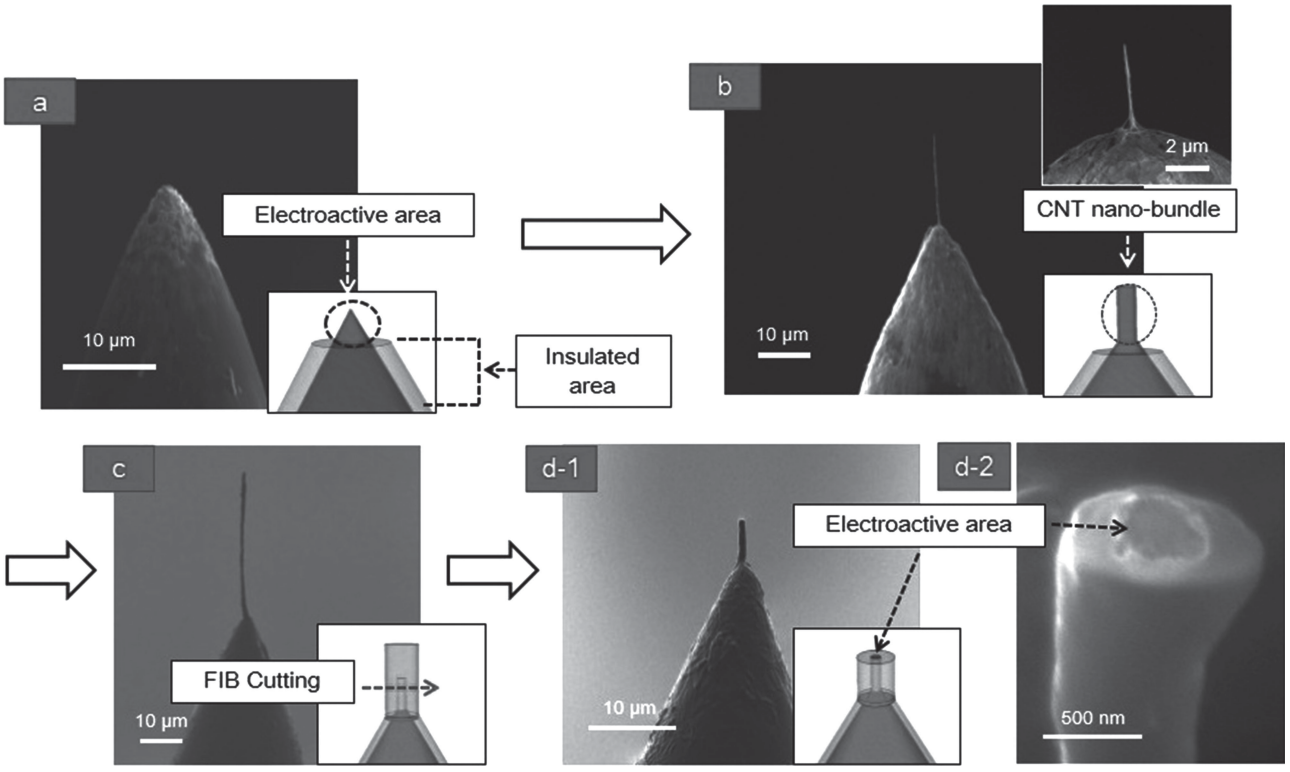

Figure 1. Scanning electron microscopy images of the carbon nanotube-modified electrode (CNE) fabrication process. a) Preparation of a conventional neural electrode (FHC Instruments, 5 MΩ). b) Attachment of a CNT nanobundle onto a conventional neural electrode. c) Insulation of the entire electrode using insulation material (parylene-C). d) Focused ion beam cutting of the apex of the nanobundle.

Nanoscale electrodes, which have a small electroactive area of sub-micrometer dimensions, have been used as individual nanoelectrodes and in nanoelectrode arrays or nanoelectrode ensembles.[28,29] Nanoelectrodes, with their high spatial resolution,[30,31] provide a better signal-to-noise ratio (SNR) because of their faster radial diffusion flux and enhanced detection limits for electrochemical and biological applications.[32,33] However, until now, no study has tried to fully exploit their ability to detect neural firing in a mouse brain in vivo.

In this study, we report the successful fabrication of CNT-modified electrodes (CNEs) based on CNT nanobundles as the electroactive area. The electromechanical and electrochemical characteristics of the CNEs are described, and their performance is compared with that of conventional tungsten microelectrodes for extracellular acute recording in vitro and in vivo. The results demonstrate the superiority of CNEs over conventional tungsten microelectrodes with respect to acute recording efficiency.

2. Results and Discussion

2.1. Electromechanical Characterization of CNEs

Figure 1a–d illustrates the CNE fabrication process. First, a CNT nanobundle was fabricated on the tip of a conventional tungsten microelectrode. The CNT nanobundle was made parallel to the direction of the microelectrode to prevent breakage during insertion of the CNE into the brain. It had a uniform diameter of approximately 400 nm along the length. The thickness of the insulating material, parylene, was about 200 nm. After cutting by the focused ion beam (FIB) process, the length of the CNT nanobundle was about 10 μm.

The contact area between the CNT nanobundle and the tungsten tip was large because many CNTs were deposited around the tungsten tip, similar to roots of a tree (Figure 1b). The conductance of the CNT nanobundle was confirmed by a two-terminal measurement between a CNT nanobundle and a fresh tungsten tip (Figure S1, Supporting Information). The linear *I–V* curve of the electrode indicated that the electrode had conductive and ohmic characteristics.

The complete insulation of the sides of a CNE is important for high selectivity to individual neurons in the brain. To test whether the CNEs had leakage or problems due to incomplete passivation, two experiments were conducted. First, the cyclic voltammetric (CV) response of the insulated CNT nanobundle was measured before the FIB step. The CV response of the insulated CNT nanobundle showed that there was no detectable redox electrochemistry (Figure S2b, Supporting Information), demonstrating that there were no pinholes in the insulating layer. Next, after the apex of the CNT nanobundle was exposed by the FIB process, gold nanoparticles were electrodeposited on the electrode. Gold growth was observed only at the apex of the CNE, whereas the stem areas remained clean and gold-free, indicating that the CNE was exposed only at the tip apex (Figure S2d, Supporting Information). These results establish

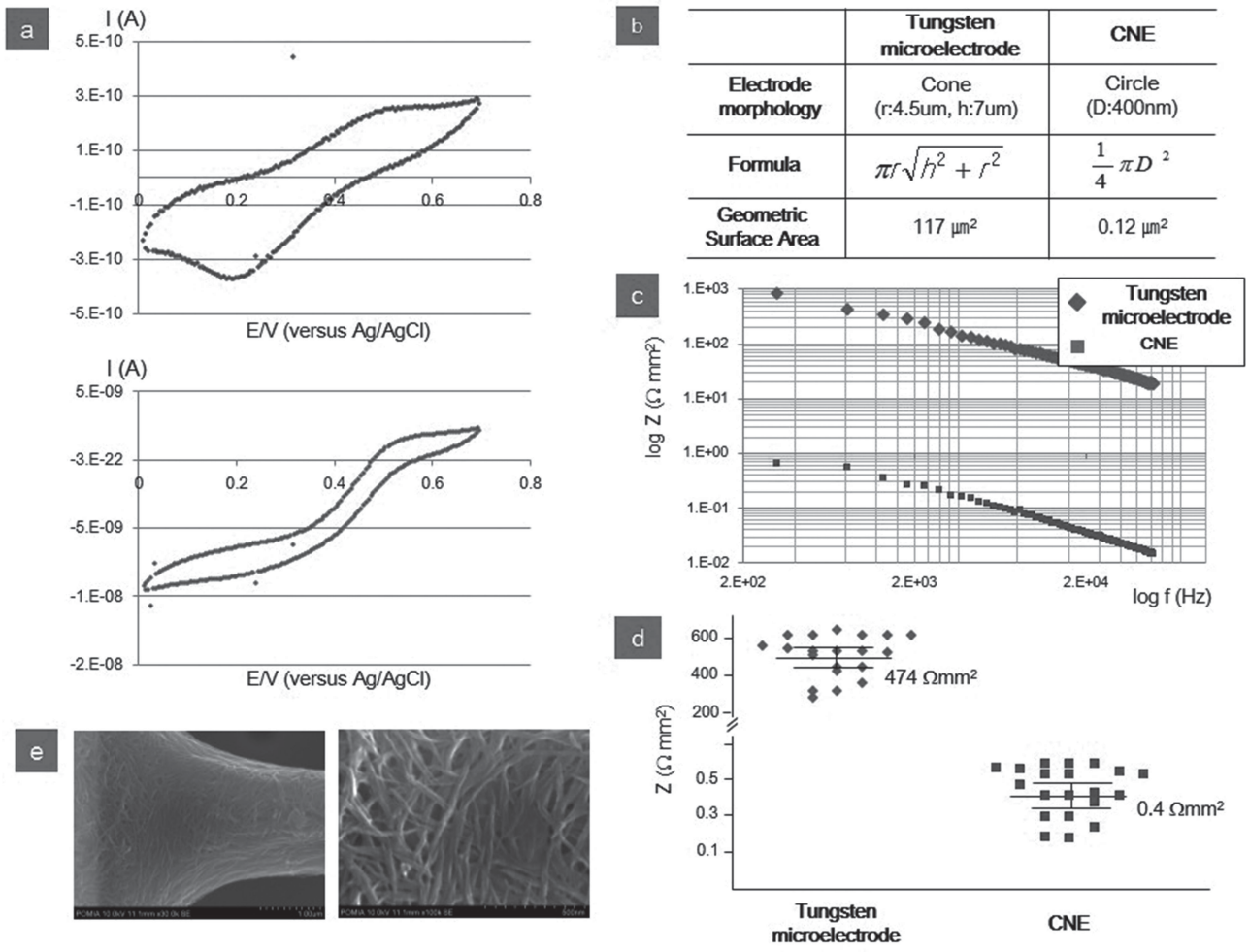

Figure 2. Electrochemical characterization of the carbon nanotube-modified electrodes (CNEs). a) Cyclic voltammetry scan of CNE and bare CNT nanobundle immersed in 20×10^{-3}M $K_3Fe(CN)_6$ in a background of 500×10^{-3}M KCl solution (scan rate: 100 mV s^{-1}), Cyclic voltammograms of CNE (upper) and cyclic voltammograms of CNT nanobundle (down). b) The formula to calculate the surface area of the electrodes was obtained from Robinson.[34] c) The impedance of tungsten microelectrode and CNE at 0.1–10 kHz. d) The impedances of the tungsten microelectrodes and CNEs at 1 kHz. ($n = 20$). e) Scanning electron microscopy images of the CNT nanobundle.

that the sides of the CNE were fully insulated and that the CNE had an electroactive area only at the tip apex.

2.2. Electrochemical Characterization of CNEs

To rule out the possibility of metal ion doping of the tip apex during FIB, and to study the electrochemical activities of the opened surface, the electrochemical response of the CNEs was compared with that of a bare CNT nanobundle prior to parylene coating. **Figure 2**a shows the measurements from CNEs in solution (red dots in upper panel) and the measurements from CNT nanobundles in solution (blue dots in lower panel). The redox peaks of the CNEs and CNT nanobundles were very similar. This finding excludes the possibility of metal ion doping and shows that the tip apex of CNEs had electrochemically active CNT species.

The impedance of neural electrodes is one of the important characteristics for neural recording because high-impedance electrodes are thought to have a lower SNR and higher signal loss in noise. The surface area of electrodes is also important for neural recording because electrodes having a large surface area generally lose selectivity and create tissue damage during insertion.[19] Recently, surface modification technologies using conducting polymers[35,36] or CNTs[19] have been applied to improve electrode impedance by increasing the ESA while maintaining the surface area. Ideally, the neural electrodes should the lowest possible impedance while maintaining a minimal surface area to increase selectivity to individual neurons.[37]

Here, we aimed to design CNEs having a much smaller than that of tungsten microelectrodes or previous CNT electrodes.[19] The surface morphology of the tungsten microelectrodes was assumed to be a circular cone, and that of the CNEs was assumed to be a circle (Figure 2b). The impedance with respect to surface area was calculated by multiplying the impedance and the surface area. The impedance of the CNEs was much less than that of the tungsten microelectrodes at all frequencies

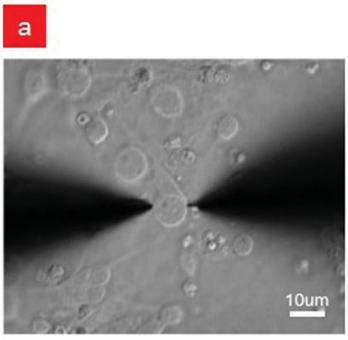

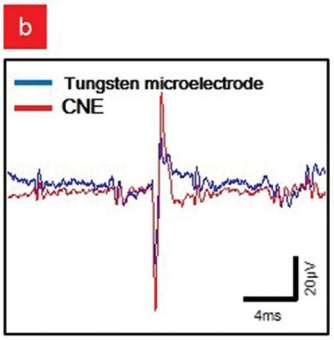

c

#	Tungsten microelectrode		CNE	
	Noise level (μV)	Signal amplitude (μV)	Noise level (μV)	Signal amplitude (μV)
1.	31	788	23	1,090
2.	32	984	25	869
3.	32	641	20	758
4.	34	1,156	20	1,341
5.	31	610	27	947

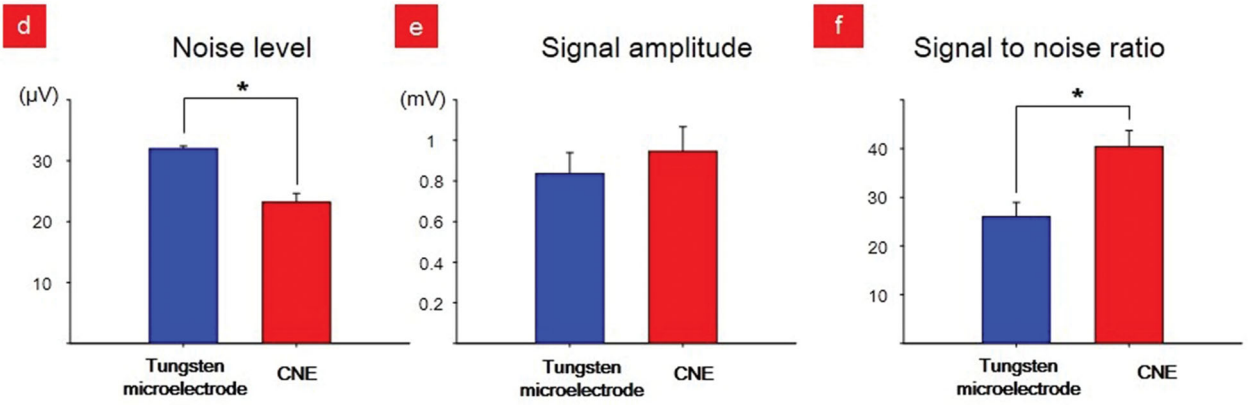

Figure 3. Acute extracellular recording of a single-cell in vitro. a) Left electrode is a tungsten microelectrode and right electrode is a CNE. The two electrodes were manipulated very closely to the target cell at the same distance. b) A raw traces recorded from two electrodes. c) The values of noise level and signal amplitude in five experiments. d) Noise level of tungsten microelectrodes and CNEs. e) Signal amplitude of tungsten microelectrodes and CNEs. f) Signal-to-noise ratio (SNR) of tungsten microelectrodes and CNEs. Values were analyzed using the paired t-test, mean ± standard error, $n = 5$, $*p < 0.05$.

(0.1–10 kHz) (Figure 2c). At the biologically related frequency of 1 kHz, the average impedances of the tungsten microelectrodes and CNEs were 474 and 0.4 Ω mm^2, respectively (Figure 2d).

Our CNT nanobundle is composed of individual CNTs with relatively large spacing among the nanotubes (Figure 2e). Pores as small as 0.5 nm could affect the double-layer capacitance[38] in an aqueous electrolyte. Therefore, our CNT nanobundle has an inherently large ESA. However, the nonpolar basal plane of CNTs makes them highly hydrophobic, and thus most of the large surface area is inaccessible to aqueous solutions and cannot contribute to charge injection.[39] The CNTs used in our experiments were oxidized upon sonication in a strong acid,[21] resulting in the formation of carboxyl groups that made the surface polar and resulted in a hydrophilic CNT nanobundle.[40,41] Because the CNT nanobundle was composed of many CNTs with spaces among them, as shown in Figure 2e, we suppose that the oxidized CNT nanobundle could be wetted by the aqueous electrolyte through the opened tip apex. This means that all CNTs in the nanobundle can function as electrodes, resulting in a dramatic increase in the ESA, which yields lower impedance. Thus, the impedance with respect to surface area of the CNEs could be reduced compared with that of tungsten microelectrodes.

2.3. Acute Recording on Cultured Cells Using CNEs

To compare the extracellular recording performance of the fabricated electrode with that of a typical tungsten electrode, we recorded using the two electrodes simultaneously from the same single neuron in culture, and then compared their performances (**Figure 3**a). Figure 3b shows raw data traces recorded simultaneously from a tungsten microelectrode (blue trace) and a CNE (red trace). The two traces exhibited parallel oscillations, suggesting that they originated from the same neuron cell. The CNE trace had a lower noise level and less signal distortion compared with the tungsten microelectrode trace. The noise level of the signal from the CNEs was significantly lower than that from the tungsten microelectrodes (Figure 3d, $p = 0.0068$), and the SNR from the CNEs was significantly higher than that from the tungsten microelectrodes (Figure 3f, $p = 0.0477$). The amplitudes from the two electrodes were similar, reflecting the fact that the two electrodes were situated at the same distance from the cell (Figure 3e). The lower noise level of the CNE is attributable to the decreased impedance, which reduces thermal noise.[35] These results demonstrate that compared with tungsten microelectrodes, CNEs have better sensitivity for extracellular acute recording.

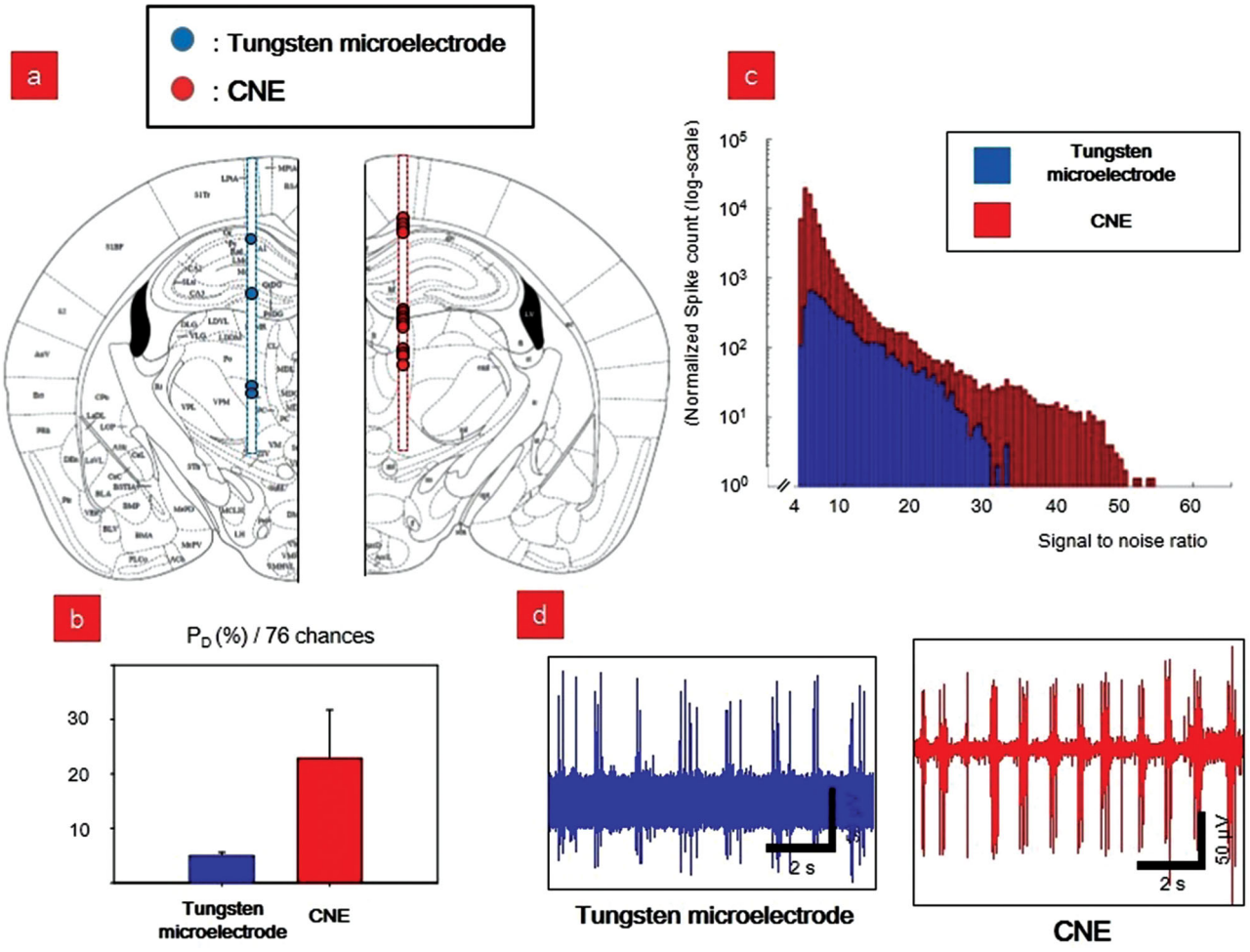

Figure 4. Spontaneous multiunit activity acute recording using two electrodes in vivo. a) The marked colored circles represent the equivalent position which the electrode could detect action potentials (AP: –1.7, ML: ±1, tungsten microelectrodes: blue circle, CNEs: red circle, $n = 5$). b) The average P_D of tungsten microelectrodes and CNEs. c) The SNR and spike number distribution of the whole traces recorded from tungsten microelectrodes and CNEs. d) A raw trace recorded from tungsten microelectrode and CNE.

2.4. Acute In Vivo Recordings Using CNEs

To compare the acute in vivo recording performance, the electrodes were inserted (anteroposterior, –1.7 mm; lateral, ±1 mm) vertically along the dorso-ventral axis of the mouse brain. Recording was carried out from 76 sequential positions each 50 μm apart, including the cortex, hippocampus, and thalamus regions of the mouse brain. The recorded APs were categorized as good (SNR >4) and fair (SNR 2–4) signals.[42] The probability of detecting good signals (P_D: SNR >4) was calculated as the ratio between the number of positions with successful signal acquisition and the total number of positions tested.

In **Figure 4**a, the blue/red lines represent the inserted traces with the tungsten microelectrodes/CNEs, and the blue/red dots indicate the positions where the two electrodes detected APs in each trial. For each of the five electrodes for at 76 positions, the average P_D of the CNEs was about five-fold that of the tungsten microelectrodes, corresponding to probabilities of 4.9% and 22.9%, respectively (Figure 4b). This means that the CNEs could detect APs more efficiently than the tungsten microelectrodes.

To evaluate the acute recording performance of tungsten microelectrodes and CNEs, the SNR and spike number distribution of the whole traces, recorded by the two electrodes, were analyzed using MATLAB (Figure 4c). Compared with tungsten microelectrodes, the CNEs had a higher SNR, which means that the CNEs showed enhanced sensitivity in acute neural recording in vivo. Moreover, the CNEs detected more spikes (or more cells), indicating that the damage to neural cells around the inserted CNEs was less than that around the tungsten microelectrodes; we assumed that the small and sharp morphology of the CNEs reduced the damage. Taken together, these findings demonstrate that nanometer-scale CNEs can enhance the signal sensitivity and improve the detection of APs in vivo.

In addition to selecting for signal over noise, the selectivity of an electrode in distinguishing among different APs is important when recording in vivo, especially when it is necessary to isolate a single unit from among multiple mixed neural signals.

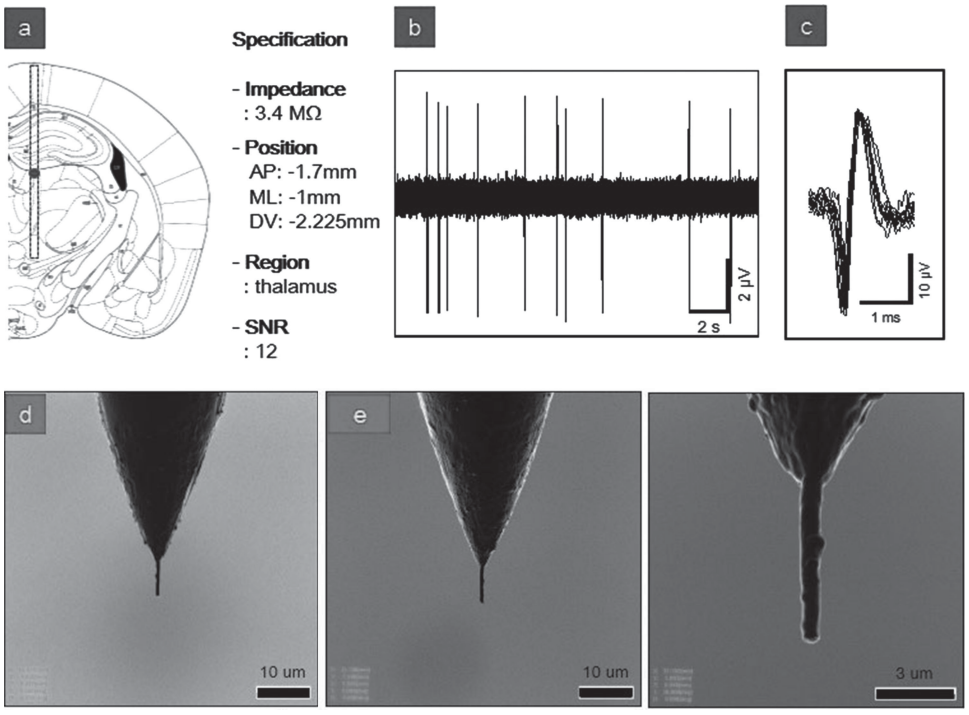

Figure 5. Single-unit acute recording using carbon nanotube-based neural electrodes (CNEs). a) The specified region where the single unit was recorded. b) Data were recorded from the CNE. c) Superimposed 10 spikes from (b). d) Scanning electron microscopy image of the carbon nanotube CNT-based neural electrode (CNE) before insertion into the mouse brain. e) Scanning electron microscopy image of the carbon nanotube CNT-based neural electrode (CNE) after removed from the mouse brain.

During acute in vivo recording (Figure 4a), CNEs having high selectivity could record a single unit twice; **Figure 5**b shows the single-unit trace recorded from CNEs. In contrast, tungsten microelectrodes having low selectivity could not record sing-units (Figure S1c, Supporting Information). Figure 5c illustrates that all signals had the same amplitude and duration, suggesting that the spikes originated from the same neural cell. The noise level was about 150 μV, and the SNR was about 4.8.

After the CNE was inserted into the mouse brain and used for recording neural signals, the CNE was washed in PBS, and SEM images were taken (Figure 5d,e). The length and diameter of the CNE were maintained at 6.6 μm and 700 nm, respectively, after the CNE was removed from the mouse brain. These findings demonstrate that the CNE was stable during insertion into the mouse brain and during the recording of neural signals.

3. Conclusions

In summary, CNEs using CNT nanobundles were developed as neural electrodes.The impedance with respect to the surface area of the CNEs was markedly smaller than that of the tungsten microelectrodes because the hydrophilic surfaces of the CNTs enhanced the electrochemical surface area. In acute in vitro extracellular recording, compared with tungsten microelectrodes, the CNEs displayed significantly reduced noise and signal distortion, and significantly increased SNR of neural firings. In acute in vivo extracellular recording, the use of increased the recording sensitivity more than five-fold compared with that of conventional tungsten microelectrodes. Furthermore, CNEs with high selectivity have a greater probability of recording single units from among multiple mixed neural signals. This is an exciting advance for neural signal recording in the field of neuroscience, and our novel modification techniques could be applied to various neural electrodes (e.g., Si electrodes, multiple-site electrodes, and tetrodes) to enhance recording sensitivity.

4. Experimental Section

Fabrication of the CNEs: CNT nanobundle can be fabricated on a sharpened tungsten tip using dielectrophoresis and surface tension.[43] Because we were interested in applying CNE as a extracellular neural electrode, CNT nanobundle was fabricated on conventional neural electrode and compared them with standard neural electrode. Conventional neural electrodes were purchased from FHC Instruments (5 MΩ; 1201 Main street, Bowdoin, ME 04287). Single-wall nanotubes (SWNTs) were produced using an arc discharge process (1.0–1.2 nm diameter and 5–20 μm length) (Hanhwa Nanotech, Seoul, South Korea),[43] and CNTs were oxidized in a strong acid with sonication for dispersion. Typically, the side of the nanobundle is insulated for high spatial resolution during electrochemical and biological sensing. Generally, parylene-C forms a biocompatible interface between the electrode and brain tissue,[37] and its vapor-deposition procedure guarantees precise thickness and pinhole-free coating of a large batch.[44] The CNT nanobundle was insulated with parylene-C (poly-dichloro-diparaxylylene). Finally, the apex of the CNT nanobundle was opened by a 30 kV gallium focused ion beam (SMI 3050, SII Nanotechnology, Inc., Japan) to a desired length.

Focused Ion Beam Process: When utilizing FIB for micro/nanostructuring, gallium doping generally occurs up to a few nanometers below the surface, resulting in a defect in the layer[45,46] and the electrode could be partially blocked by debris from FIB process.[27,47] To minimize the amount of the gallium ion induced doping and the blocking by debris, herein, the two-step FIB processing was utilized; 1) the 90 pA of probe current was adopt to open the electroactive area from the fully insulated neural electrode roughly, resulting in the open of electroactive area of the CNT nanobundle, having little slant end by the Gaussian ion beam profile. 2) The 10 pA of probe current polished the roughly opened electroactive area with the tilt angle of 2° during only 2–3 s to form the very clean and flat surface. Simultaneously, the slant end of nanobundle was eliminated. Also, this surface polishing with low current beam was essential to remove the residue, flowed down from the top surface induced by the high current ion beam of 90 pA, on the electrode surface when cross-sectioning the electrode.

Two Terminal Measurements: Two tungsten tips were placed a 10 μm apart, and an AC electric field was applied between them. CNT nanobundle was fabricated between the tips because of dielectrophoresis and surface tension. The diameter and length of the fabricated CNT nanobundle were 400 nm and 10 μm, respectively. The *I*–*V* response was measured using a semiconducting analyzer (Figure S1, Supporting Information).

Cyclic Voltammetry Measurements: The CV response of an electrode was measured in 0.02 M $K_3Fe(CN)_6$ in a background of 0.5 M KCl solution using three-electrode configuration (Modulab System, Solartron Instruments, Elmsford, NY, USA). The three-electrode cell was composed of a Ag/AgCl reference electrode, a Pt counter electrode, and a W/ or W/O CNE test electrode. A scan rate of 100 mV s^{-1} was used between potential limits of –0.8 V and 0.4 V beginning at the open-circuit potential and sweeping in a positive direction. Several cycles were swept before recording to assure that the electrode attained a stable state.

Gold Nanoparticle Coating: Au nanoparticles were electrodeposited on the CNE using a electrodeposition. Sweeping potential was applied between –0.1 and +1.5 V versus a Ag/AgCl electrode in an aqueous solution containing 1–5 × 10^{-3} M $HAuCl_4$ $4H_2O$ and 500 × 10^{-3} M HBO_3 solution.

Impedance Measurements: The impedance of the electrode was measured with an impedance analyzer (HP 4192A, Hewlett-Packard, Palo Alto, CA, USA) between the electrode and a Ag/AgCl as the reference and Pt counter electrode in phosphate-buffered saline (PBS; pH 7.4) at frequencies ranging from 0.1 to 10 kHz.

Neuron Cell Culture: Primary cultured cortical neurons for single-cell recording were used. Cortical neurons were isolated from brains of postnatal mouse pups (P1). A neural culture was prepared using the Papain Dissociation System (Worthington Biochemical Corp., Lakewood, NJ, USA) following the manufacturer's protocol. Cells were plated on poly-L-ornithine-coated cover glasses (Sigma, St. Louis, MO, USA) at a density of 2 × 10^5 cells mL^{-1} and maintained in Neurobasal A medium 1XB27, 0.5 × 10^{-3} ML-glutamine, and 1% penicillin–streptomycin (Gibco, Grand Island, NY, USA). The medium was replaced every 3 d until the study ended. Experiments were performed after day 14 (DIV14) to study fully active mature neurons. Two electrodes were positioned very close to a target cell using a patch-clamp system in artificial cerebrospinal fluid solution (123 × 10^{-3} M NaCl, 26 × 10^{-3} M $NaHCO_3$, 2.5 × 10^{-3} M KCl, 1.25 × 10^{-3} M NaH_2PO_4, 2 × 10^{-3} M $MgCl_2$_$6H_2O$, 2 × 10^{-3} M $CaCl_2$_$2H_2O$, and 10 × 10^{-3} M glucose) (Figure 3a).

Mice: Animal care and experimental procedures followed the guidelines of the Institutional Animal Care and Use Committee of the Korea Institute of Science and Technology.

In Vitro and In Vivo Signal to Noise Ratio Analysis: To estimate the signal to noise ratio, a noise threshold was established, based on the cumulative distribution of spike amplitude and unit spike peak-to-peak spike amplitude. For in vivo recordings, the noise level was set a high and low threshold corresponding to 99% of cumulative distribution of positive and negative spike amplitude, respectively. For in vitro recordings, since clear unit separation was observed, the high and low threshold detection were set to clearly distinguish the single spike observed from noise. For in vivo recordings, only spike wave form that had maximum and minimum crossing was considered, respectively, the high and low threshold within 1.5 msec. All spikes in the range low to high noise threshold was considered noise signal. The SNR in decibel (dB) was estimated for each observed spike as $20 \times \log_{10}$ [((Spike peak-to-peak amplitude))/(noise standard deviation))].

In Vitro SNR Statistical Analysis: The SNR value distribution obtained during in vitro recordings was compared using commercial tungsten electrode and CNE electrode using a Student paired t-test. Considering the low sample number, this comparison was confirmed using a non-parametric approach, the Wilcoxon signed rank test (noise level and SNR: $p = 0.0625$, signal amplitude: $p = 0.8125$).

In Vivo Action Potential Acute Recording: In vivo acute recording of CNEs was tested in the cortex, hippocampus, and thalamus regions of the mouse brain. Experiments were performed with B6 male mice under urethane anesthesia (1.5 g kg^{-1}). The animals were anesthetized with an intraperitoneal dose and then head-fixed into a standard stereotaxic surgical apparatus. The electrodes were lowered at 50 μm intervals from 200 to 4000 μm (anteroposterior, –1.7 mm and lateral, ±1 mm), and neural signals were recorded for 1 min at each step. The electrodes were lowered slowly using a microcontroller system at a 5 μm s^{-1} insertion rate (0.1 μm resolution).

In Vivo SNR and Spike Number Distribution: The SNR value distribution of the commercial tungsten microelectrodes and CNEs was estimated using the pooled data of each recordings single spike SNR value.

Supporting Information

Supporting Information is available from the Wiley Online Library or from the author.

Acknowledgements

The authors thank Chung-Soo Kim for the comment on FIB fabrication and J. Park for assistance in animal care. This work was supported by the National Research Foundation of Korea (NRF) grant funded by the Korea government (MEST) (No. 2012R1A2A2A06047424). This work was supported by the Research Center Program of IBS (Institute for Basic Science) in Korea.

Received: May 14, 2013
Revised: June 28, 2013
Published online: August 15, 2013

[1] P. K. Campbell, K. E. Jones, R. A. Normann, *Biomed. Sci. Instrum.* **1990**, *26*, 161.
[2] P. K. Campbell, K. E. Jones, R. J. Huber, K. W. Horch, R. A. Normann, *IEEE Trans. Biomed. Eng.* **1991**, *38*, 758.
[3] K. A. Moxon, N. M. Kalkhoran, M. Markert, M. A. Sambito, J. L. McKenzie, J. T. Webster, *IEEE Trans. Biomed. Eng.* **2004**, *51*, 881.
[4] K. A. Moxon, S. C. Leiser, G. A. Gerhardt, K. A. Barbee, J. K. Chapin, *IEEE Trans. Biomed. Eng.* **2004**, *51*, 647.
[5] D. Pellinen, T. Moon, R. Vetter, R. Miriani, D. Kipke, *Conf. Proc. Annu. Int. Conf. IEEE Eng. Med. Biol. Soc.* **2005**, *5*, 5272.
[6] W. Jensen, K. Yoshida, U. G. Hofmann, *IEEE Trans. Biomed. Eng.* **2006**, *53*, 934.
[7] K. C. Cheung, P. Renaud, H. Tanila, K. Djupsund, *Biosens. Bioelectron.* **2007**, *22*, 1783.
[8] M. A. Wilson, B. L. McNaughton, *Science* **1993**, *261*, 1055.
[9] B. L. McNaughton, J. O'Keefe, C. A. Barnes, *J. Neurosci. Methods* **1983**, *8*, 391.

[10] C. M. Gray, P. E. Maldonado, M. Wilson, B. McNaughton, *J. Neurosci. Methods* **1995**, *63*, 43.
[11] D. A. Henze, Z. Borhegyi, J. Csicsvari, A. Mamiya, K. D. Harris, G. Buzsáki, *J. Neurophysiol.* **2000**, *84*, 390.
[12] M. Jog, C. Connolly, Y. Kubota, D. Iyengar, L. Garrido, R. Harlan, A. Graybiel, *J. Neurosci. Methods* **2002**, *117*, 141.
[13] T. G. Yuen, W. F. Agnew, *Biomaterials* **1995**, *16*, 951.
[14] M. A. L. Nicolelis, D. Dimitrov, J. M. Carmena, R. Crist, G. Lehew, J. D. Kralik, S. P. Wise, *Proc. Natl. Acad. Sci. U.S.A.* **2003**, *100*, 11041.
[15] P. J. Rousche, R. A. Normann, *J. Neurosci. Methods* **1998**, *82*, 1.
[16] Q. Bai, K. D. Wise, *IEEE Trans. Biomed. Eng.* **2001**, *48*, 911.
[17] S. F. Cogan, *Annu. Rev. Biomed. Eng.* **2008**, *10*, 275.
[18] B. P. Ruddy, *Master's Thesis*, Massachusetts Institute of Technology, **2006**.
[19] E. W. Keefer, B. R. Botterman, M. I. Romero, A. F. Rossi, G. W. Gross, *Nat. Nanotechnol.* **2008**, *3*, 434.
[20] S. Banerjee, M. G. C. Kahn, S. S. Wong, *Chem. Eur. J.* **2003**, *9*, 1898.
[21] T. An, K. S. Kim, S. K. Hahn, G. Lim, *Lab. Chip* **2010**, *10*, 2052.
[22] A. Meulemans, B. Poulain, G. Baux, L. Tauc, D. Henzel, *Anal. Chem.* **1986**, *58*, 2088.
[23] T. Abe, Y. Y. Lau, A. G. Ewing, *J. Am. Chem. Soc.* **1991**, *113*, 7421.
[24] P. E. M. Phillips, G. D. Stuber, M. L. A. V. Heien, R. M. Wightman, R. M. Carelli, *Nature* **2003**, *422*, 614.
[25] Y. Qiao, J. Chen, X. Guo, D. Cantrell, R. Ruoff, J. Troy, *Nanotechnology* **2005**, *16*, 1598.
[26] A. Kueng, C. Kranz, B. Mizaikoff, A. Lugstein, E. Bertagnolli, *Appl. Phys. Lett.* **2003**, *82*, 1592.
[27] D. P. Burt, N. R. Wilson, J. M. R. Weaver, P. S. Dobson, J. V. Macpherson, *Nano Lett.* **2005**, *5*, 639.
[28] H. Shi, J. I. Yeh, *Nanomedicine* **2007**, *2*, 587.
[29] H. Shi, T. Xia, A. E. Nel, J. I. Yeh, *Nanomedicine* **2007**, *2*, 599.
[30] C. Jk, S. L. C. Rm, *J. Am. Chem. Soc.* **1999**, *121*, 3779.
[31] K. Yum, H. N. Cho, J. Hu, M.-F. Yu, *ACS Nano* **2007**, *1*, 440.
[32] M. Rw, *Chem. Rev.* **2008**, *108*, 2688.
[33] R. L. McCreery, *Chem. Rev.* **2008**, *108*, 2646.
[34] D. A. Robinson, *Proc. IEEE* **1968**, *56*, 1065.
[35] M. R. Abidian, K. A. Ludwig, T. C. Marzullo, D. C. Martin, D. R. Kipke, *Adv. Mater.* **2009**, *21*, 3764.
[36] M. R. Abidian, J. M. Corey, D. R. Kipke, D. C. Martin, *Small* **2010**, *6*, 421.
[37] G. E. Loeb, R. A. Peck, J. Martyniuk, *J. Neurosci. Methods* **1995**, *63*, 175.
[38] E. Frackowiak, F. Béguin, *Carbon* **2001**, *39*, 937.
[39] A. O. Fung, C. Tsiokos, O. Paydar, L. H. Chen, S. Jin, Y. Wang, J. W. Judy, *Nano Lett.* **2010**, *10*, 4321.
[40] J. B. Donnet, M. Brendle, T. L. Dhami, O. P. Bahl, *Carbon 24*, 757.
[41] C. Vix-Guterl, M. Couzi, J. Dentzer, M. Trinquecoste, P. Delhaes, *J. Phys. Chem. B* **2004**, *108*, 19361.
[42] S. Suner, M. R. Fellows, C. Vargas-Irwin, G. K. Nakata, J. P. Donoghue, *IEEE Trans. Neural Syst. Rehabil. Eng. Publ. IEEE Eng. Med. Biol. Soc.* **2005**, *13*, 524.
[43] T. An, W. Choi, E. Lee, I. Kim, W. Moon, G. Lim, *Nanoscale Res. Lett.* **2011**, *6*, 306.
[44] G. E. Loeb, M. J. Bak, M. Salcman, E. M. Schmidt, *IEEE Trans. Biomed. Eng.* **1977**, *BME-24*, 121.
[45] G. Hobler, W. J. MoberlyChan, D. P. Adams, M. Aziz, T. Schenkel, Fundamentals of Focused Ion Beam Nanostructural Processing: Below, At, and Above the Surface **2007**.
[46] C.-S. Kim, S.-H. Ahn, D.-Y. Jang, *Vacuum* **2012**, *86*, 1014.
[47] A. J. Wain, D. Cox, S. Zhou, A. Turnbull, *Electrochem. Commun.* **2011**, *13*, 78.